Published in final edited form as:
Neuron. 2013 July 10; 79(1): 69–81. doi:10.1016/j.neuron.2013.05.018.

A prestin motor in chicken auditory hair cells

Maryline Beurg[1,2], **Xiaodong Tan**[1], and **Robert Fettiplace**[1]

[1]Department of Neuroscience, University of Wisconsin Medical School, Madison, WI 53706

[2]INSERM U587, Université Bordeaux Segalen, CHU, Bordeaux, France

Abstract

Active force generation by outer hair cells (OHCs) underlies amplification and frequency tuning in the mammalian cochlea but whether such a process exists in non-mammals is unclear. Here we demonstrate that hair cells of the chicken auditory papilla possess an electromechanical force generator in addition to active hair bundle motion due to mechanotransducer channel gating. The properties of the force generator, its voltage-dependence and susceptibility to salicylate, as well as an associated chloride-sensitive non-linear capacitance, suggest involvement of the chicken homolog of prestin, the OHC motor protein. The presence of chicken prestin in the hair cell lateral membrane was confirmed by immunolabeling studies. The hair bundle and prestin motors together create sufficient force to produce fast lateral displacements of the tectorial membrane. Our results imply that the first use of prestin as a motor protein occurred early in amniote evolution and was not a mammalian invention as is usually supposed.

INTRODUCTION

In the evolutionary drive to expand the frequency range of hearing, the avian auditory papilla lies between the primitive organ of the turtle and the structurally complex mammalian cochlea. This transformation can be mapped onto the audible frequency limits of these classes ranging from 600 Hz in the turtle, 5 - 10 kHz in birds to over 100 kHz in some mammals (Manley, 2000). The bird auditory papilla still employs electrical tuning like the turtle (Fuchs et al., 1988; Tan et al., 2013) but also exhibits mechanical tuning of the basilar membrane (Gummer et al., 1987) similar to mammals. Furthermore, avian auditory hair cells can be divided into two sub-types, tall hair cells (THC) and short hair cells (SHC) (Takasaka and Smith, 1971; Hirokawa, 1978), which are analogous to mammalian inner and outer hair cells based on their location and innervation. SHCs like their mammalian counterpart are situated more abneurally and innervated mainly by efferent rather than afferent fibers (Fischer, 1992).

Because of the similarities, it has been conjectured that SHCs possess a mechanism to confer amplification and boost frequency selectivity (Manley and Köppl, 1998; Köppl, 2011) just as the prestin-based somatic motility is thought to do in OHCs (Zheng et al., 2000; Dallos, 2008; Ashmore, 2008). Generation of an active force output is consistent with otoacoustic emissions that have been recorded in some avian species as they have in mammals (Manley

Address correspondence to: Robert Fettiplace, 185 Medical Sciences Building, 1300 University Avenue, Madison, WI 53706. Tel: 608-262-9320; FAX: 608-265-5512. fettiplace@wisc.edu.

and Köppl, 1998). However, there is no evidence for the occurrence of prestin in SHCs (He et al., 2003; Schaechinger and Oliver, 2007). Instead, there has been promulgation of the idea that non-mammalian hair cells exploit active hair bundle motility driven by gating of the mechanotransducer (MT) channels to amplify extrinsic stimuli (Manley and Köppl, 1998; Hudspeth et al., 2000; Köppl, 2011). Detailed models have been proposed to support such a mechanism in birds (Choe et al., 1998; Sul and Iwasa, 2009). Active hair bundle movements have been documented in both turtles (Crawford and Fettiplace, 1985; Ricci et al., 2000) and frogs (Benser et al., 1996 Martin et al., 2003), where they stem from force generation due to gating and fast adaptation of the MT channels. However, there has been no systematic study of this process in chicken hair cells.

The goal of the present work was to address the role of avian SHCs by directly measuring the electromechanical properties of their hair bundles. We demonstrate that SHCs possess an electromechanical force generator with properties akin to prestin in addition to active bundle motion attributable to MT channel gating. The two mechanisms together create sufficient force to produce lateral displacements of the tectorial membrane, which can be transmitted to THCs not overlying the basilar membrane. We show that prestin is present in the hair cell membrane, our results implying that transformation of the SLC26A5 anion exchanger into a motor protein (Schaechinger and Oliver, 2007; Tan et al., 2011) was an early development in amniote evolution and not a mammalian innovation.

RESULTS

Voltage-induced bundle movements

Maximal MT currents were evoked in SHCs by hair bundle displacements of ± 100 nm (Fig. 1B) elicited by a sinusoidal fluid jet stimulus. Movements of free-standing hair bundle (Fig. 1A) were quantified by projecting an image of the bundle tip onto a photodiode pair (Crawford and Fettiplace, 1985) from which the current-displacement relationship was constructed and fitted with a single Boltzmann equation (see Methods). The maximum current for 17 SHCs was 0.60 ± 0.24 nA (mean ± SD) at a holding potential of −84 mV, and the 10 to 90 percent working range was 52 ± 18 nm (d, the fractional distance along the papilla from the apex = 0.36 to 0.42; T = 33°C). In such SHCs, depolarizing voltage steps evoked negative deflections of the free-standing bundles away from their tallest edge (Fig. 1C), the polarity being the same as would close the MT channels. Frequently the response was accompanied by a positive overshoot at the end of the stimulus (Fig. 1C, 2A, 2B). The depolarizing step also evoked an outward membrane current carried in SHCs by Ca^{2+} activated and A-type inactivating K^+ channels, the latter being characteristic of SHCs (Murrow, 1994; Tan et al., 2013). The magnitude of the voltage-induced displacement was up to 50 nm (mean = 34 ± 12 nm in 17 SHCs, d = 0.35 – 0.45) and was thus comparable to the working range of the transduction mechanism. The displacement was graded with the size of the voltage step and was significant even if a flexible fiber was attached to the bundle (Fig. 1D), which allowed us to determine the force generated. The largest displacement observed was 46 nm (when working against a fiber of stiffness 1.2 mN/m), equivalent to a peak force of 55 pN.

The hair bundle displacements were unusual in two respects, their polarity and biphasic nature. Such voltage-induced displacements of free-standing hair bundles were characterized in turtle auditory hair cells where they were uniformly positive and linked to adaptation of the MT channels (Ricci et al., 2000). They are thought to arise because depolarization reduces the Ca^{2+} influx and shifts the current-displacement relationship of the MT channels negative, hence producing a compensatory positive hair bundle movement towards the bundle's tallest edge. In SHCs, application of MT channel blockers FM1-43 (Gale et al., 2001) or dihydrostreptomycin (not illustrated) revealed a sustained negative displacement

(Fig. 2A). FM1-43 was preferred as a blocker of the MT channel because it was equally effective at positive and negative membrane potentials (Gale et al., 2001), whereas the block by dihydrostreptomycin is reduced at positive potentials (Marcotti et al., 2005). The negative component was reduced or abolished by application of 10 mM Na^+ salicylate (Fig. 2B), an agent that had no effect on the magnitude of the MT current (Fig. 2C). The characteristics of the negative component were obtained after application of 7.5 μM FM1-43. The component was monophasic and in eight SHCs had a peak amplitude of −51 ± 14 nm and developed with an onset time constant of 0.68 ± 0.22 ms. The amplitude of the monophasic component was reduced by 0.81 ± 0.08 (n = 8) in 10 mM Na^+ salicylate. We conclude that the hair bundle movements are composed of two processes of opposite polarity (the positive one blocked by FM1-43 and the negative one by Na^+ salicylate), their biphasic nature originating from differences in the kinetics of the components. The one blocked by salicylate, with a time constant less than 1 ms, was faster than the other component attributable to the MT channels. In general, it was also larger and less metabolically vulnerable than the positive component, and was almost always present. The effects of FM1-43 and salicylate on the hair bundle movements were confirmed to be fully reversible where examined (Fig. 3C, Fig. 4E), showing that they were not due to non-specific cell deterioration.

The voltage-induced bundle motion was not confined to the SHCs and was also seen in THCs. The bundle displacement was −25 ± 13 nm in 10 THCs that had maximum MT currents of 0.47 ± 0.21 nA. As with that in SHCs, the motion was negative (away from the tallest edge of the bundle) and it too could be decomposed into two components by application of the blocking agents (Fig. 3A). Moreover, both components were graded in amplitude with membrane potential. The relationship between the negative bundle movement, ΔX, and membrane potential, V, in the presence of FM1-43 was fit with a Boltzmann equation, $\Delta X = \Delta X_{max} /(1 + \exp(-(V-V_{0.5})/\alpha))$ with $V_{0.5}$ = 10 mV, α = 37 mV and ΔX_{max} = −70 nm. The fitting parameters, $V_{0.5}$ = 10 mV and valence = 26.4/ α = 0.71, were comparable to those derived from fits to the non-linear capacitance results (Fig. 5A). THCs were not extensively studied because their bundles were less bright and more difficult to image due to their location over the neural limb. Nevertheless there is no evidence that the motor properties are unique to the SHCs.

Evidence for a prestin-like motor

The block of the voltage-dependent bundle displacement by 10 mM Na^+ salicylate is reminiscent of its effects on prestin and the somatic contractions of OHCs, which are blocked by the same concentration (Tunstall et al., 1995). However, salicylic acid is a weak base, traversing membranes in an uncharged form and dissociating intracellularly to release H^+ ions that acidify the cytoplasm. As a consequence it could in theory exert a non-specific effect due to the pH reduction. As an anti-inflammatory agent, it also blocks conversion of arachidonic acid to prostanoids (Amman and Peskar, 2002). We searched extensively for an effect of salicylate on the MT channels and found nothing of significance. When it was applied over an extended period of time, no change in the peak amplitude of the MT current was observed (Fig. 4A, C) despite the salicylate reversibly reducing the voltage-evoked bundle movement (Fig. 4E), nor was there any change in the current-displacement relationship (Fig. 4B). This lack of effect was observed on multiple cells, whether stimulated with a fluid jet or a piezoelectric actuator driving a stiff glass probe, and independent of the mode of application of the salicylate, by either local or bath perfusion. Measurements on 12 SHCs gave a mean MT current of 0.39 ± 0.17 nA in controls and 0.38 ± 0.17 nA after administering 10 mM Na^+ salicylate, there being no significant difference between the two means (two-tailed Student t test, $p = 0.71$). With stiff probe stimulation, fast adaptation of the MT channels was observed and was unaffected by salicylate (Fig. 4D). These

observations all argue that salicylate is not acting via inhibition of MT channel gating. The possibility remains that its action is still linked to acidification of the cytoplasm, which has been reported to drop from 7.4 to 6.9 when OHCs are exposed to 5 mM extracellular Na^+ salicylate (Tunstall et al., 1995). When experiments were performed with patch electrodes containing an internal solution that had been acidified to pH 6.5 (waiting at least five minutes after achieving the whole-cell condition so the intracellular solution matches that of the pipette); the negative voltage-induced bundle movement persisted but was still reduced by 10 mM Na^+ salicylate (Fig. 4F). This suggests that acidification is not the main mode of salicylate action on SHCs.

Besides its susceptibility to salicylate, another property of the prestin motor is the accompanying charge movement during voltage activation which is manifested as a non-linear capacitance (Tunstall et al., 1995; Santos Sacchi et al., 1998). A non-linear capacitance was observed in SHCs and was measured as the difference, ΔC_m, between the capacitance in the absence and presence of 10 mM Na^+ salicylate (Fig. 5A). ΔC_m displayed a bell-shaped increase in capacitance superimposed on a linear capacitance of 5.6 ± 0.6 pF (n = 8; d = 0.39 -0.41). Fits to the non-linear capacitance using equation 1 gave the voltage at peak capacitance $V_{0.5}$, of 6 ± 15 mV and a valence, z, of 0.64 ± 0.14 (n = 8). To demonstrate the reversibility of salicylate, the capacitance-voltage relationship in the presence of blocker was subtracted from the control capacitance-voltage relationship prior to its application (Fig. 5A, filled symbols) and on washout (Fig. 5A, open symbols). The two non-linear capacitance plots had similar peak capacitance (22 fF/pF before and after) and valence (z = 0.71 before and 0.63 after), but there was an 18 mV positive shift in $V_{0.5}$ on recovery. A non-linear capacitance has previously been observed in HEK cells transfected with chicken prestin (Tan et al. 2011). The non-linear capacitance in chicken SHCs, similar to that in mammalian OHCs, was sensitive to intracellular chloride concentration (Oliver et al., 2001; Ashmore, 2008). Recordings with an intracellular solution containing 20 mM Cl^-showed that the activation range was shifted in the depolarized direction by about 50 mV compared to the control 161 mM Cl^- (Fig. 5B). In low intracellular Cl^-, $V_{0.5}$, = 56 ± 10 mV and z = 0.62 ± 0.03 (n = 5). The values for valence, z, in the normal and low intracellular Cl^- were not significantly different (two-tailed Student t test, p = 0.52). The maximum ΔC_m recorded was 180 fF from which a maximum charge movement was calculated as 29 fC (mean = 18 ± 7 fC, n = 8). Although this is small compared to the values reported for OHCs (2 to 3 pC for low-frequency cells; Santos Sacchi, 1991; Ashmore, 2008), the SHC membrane area is much smaller than that of the elongated OHCs. The lateral membrane for a SHC of 9 μm length and 7 μm diameter (d = 0.4; Tan et al., 2013) is ~200 μm^2, and therefore the maximum charge density is ~900 $e/\mu m^2$ compared to 10,000 $e/\mu m^2$ in mammalian OHCs (Mahendrasingam et al., 2010).

If a prestin-like motor is operational in SHCs, then it is likely to act at the cell body and be mechanically coupled to neighboring hair cells. Voltage-induced hair bundle displacements were measured in one SHC and were then determined in the hair bundle of a nearby cell located along the transverse axis of the papilla. The fluid jet was repositioned from the patch-clamped hair cell to the adjacent cell to deflect that bundle and establish the polarity of the secondary bundle's photocurrent, the intensity of which was calibrated independently of the primary bundle. In all SHCs studied, depolarization of the primary cell induced displacement of the hair bundle of its neighbor (Fig. 5C, 5D) and the motion was of opposite polarity to that in the primary cell; i.e. the bundle always moved towards its tallest edge. Directly imaging the patch pipette showed that there was no movement of the pipette during the depolarizing voltage step which might have contributed to motion of the second cell. The ratio of displacements of the secondary to primary hair bundle was 0.37 ± 0.05 (n = 4) when the peak deflection in the primary was 21 ± 8 nm. This observation implies that force generation originates from the cell body as would be expected for prestin.

Flexible fiber stimulation

The phenomena reported so far were observed in free-standing hair bundles in cells subjected to large depolarizing steps. A more functionally relevant mode of stimulation is to deflect the hair bundle with force stimuli to investigate the interaction between the two motors. In five SHCs, forces administered with a glass fiber more compliant than the bundle evoked an initial deflection followed by fast recoil (Fig. 6A). The recoil was observed only with shorter stiffer fibers presumably because it was less filtered by the mechanical time constant of fiber, the product of its compliance and viscous drag. The recoil has been observed in both frog saccular hair cells (Howard and Hudspeth, 1988; Benser et al., 1996, where it has been termed an 'evoked mechanical twitch', and in turtle auditory hair cells where its kinetics mirror fast adaptation of the MT current (Ricci et al., 2000). The 'recoil' is therefore a negative hair bundle motion linked to closing of the MT channels and presumably triggered, as is adaptation, by the increase in intracellular Ca^{2+} on channel opening. In contrast, the component of voltage-induced hair bundle motion sensitive to MT channel blockers is in the positive direction (Fig. 2) and is generated by a reduction in intracellular Ca^{2+} with large depolarization (see Ricci et al., 2000; Fig. 12). The size of the recoil increased with MT channel open probability for smaller force stimuli and then decreased at larger ones and a plot of its amplitude against the MT current displayed a Gaussian variation (Fig. 6C). The greatest force generation by the MT channel gating mechanism occurs when half the MT channels are open (Markin and Hudspeth, 1995) which is approximately the case for the cell shown (Fig. 6C). The current-displacement relationship in this cell had a working range of 33 nm; if corrected for the fact that the probe was not at the tip of the bundle, the working range increased to 57 nm (Fig. 6D).

Under current-clamp recording, when the SHC produced a receptor potential, the size of the bundle's recoil increased monotonically with stimulation amplitude (Fig. 6B, 6C). The depolarization produced an extra 25 nm of negative movement (the difference between the filled and dashed lines in Fig. 6C at the maximum response). The kinetics of the recoil in current-clamp were slightly slower (decay time constant = 1.14 ± 0.16 ms, n = 5) compared to those in voltage-clamp (decay time constant = 0.72 ± 0.14 ms, n = 4; significantly different from current clamp, $p < 0.005$), the latter value probably being limited by the viscous drag on the fiber and hair bundle. It seems plausible that the extra negative motion is attributable to the prestin-like motor recruited by the depolarizing receptor potential. Consistent with this idea, depolarization to +10 mV in this cell produced about 25 nm of negative movement (away from the tallest edge; not illustrated). We suggest that the two motors act with the same polarity when the bundles are stimulated near the resting potential and can sum to produce a larger negative feedback. There was no evidence in this or other SHCs for oscillations in bundle motion at the cell's resonant frequency as observed in the turtle (Crawford and Fettiplace, 1985); an evoked 80 nm mechanical oscillation was previously reported in chicken hair cells in the absence of electrical recording (Hudspeth et al., 2000).

Two other pieces of information can be garnered from the flexible fiber stimulation. Firstly, when the fiber was attached to the hair bundle, depolarization would still deflect the bundle, which enabled calculation of the force generated by the process (Fig. 1D). In four SHCs, depolarizing voltage steps to membrane potentials of +10 to +30 mV produced 31 ± 12 nm of movement when working against a flexible fiber of stiffness 1.2 mN/m; the force generated was 37 ± 14 pN. The largest force observed was 55 pN. Secondly, the force-displacement relationship yielded a stiffness value for the hair bundle. The relationship was usually close to linear but in a few cases there was evidence of the non-linearity described previously (Howard and Hudspeth, 1988). The stiffness for small displacements (measured under hair cell voltage-clamp) showed substantial variation from cell to cell ranging from 1.6 mN/ m up to 25 mN/m with a mean of 8.6 ± 8.9 mN/m (n = 7; $d = 0.35 – 0.43$). The

variation probably reflects different sites of attachment of the fiber from the bundle tip, the apparent stiffness being the square of the distance from the bottom of the bundle (Crawford and Fettiplace, 1985). The exact attachment point was difficult to measure accurately but the tip of the fiber was usually placed behind the shortest row of stereocilia or on the rake and was thus attached between a third and half way down the bundle from the top, in which case the stiffness is increased between 2.3-fold and 4-fold. Assuming an average of these two values, the expected stiffness for forces applied at the tip are approximately one third of those measured; i.e., ~3 mN/m. Measurements were also made on THC bundles for which a stiffness measurement of 4.4 ± 1.2 mN/m (n = 6) was obtained; if the same correction is applied for fiber placement the stiffness is reduced to 1.5 mN/m. These stiffness values are larger than those reported for isolated chicken hair cells (0.5 mN/m; Szymko et al., 1992) and for turtle hair bundles (0.6 – 1.2 mN/m; Crawford and Fettiplace, 1985; Ricci et al., 2000). Chicken hair bundle at the location assayed have twice the number of stereocilia (~110; Tilney and Saunders, 1983) compared to turtle hair cells, which should make them stiffer.

Force transmission by the tectorial membrane

The hair bundles of SHCs *in vivo* are constrained by tight connections to a tectorial membrane. An important question about force generation by hair bundles is whether it is functionally significant when operating against the mass and stiffness of the tectorial membrane. To address the question, we used an isolated basilar papilla in which the tectorial membrane was left in place and we electrically stimulated the hair cells *en masse* by passing extracellular currents across the papilla (see Methods; Bozovic and Hudspeth, 2003). In these experiments, the tectorial membrane was more than 10 μm thick (mean = 10.9 ± 2.9 μm, N= 5), and evidence that it remained intact included that it was still attached to the supporting cells abneural of the SHCs and that its transverse fibers (Fig. 7A middle image) were undisturbed and ran close to the tops of the hair bundles. To monitor tectorial membrane motion, 3-μm silica beads were dispersed across the top of the membrane and their lateral displacement monitored by photodiode imaging similar to the method applied to the bundles (Fig. 7A). Extracellular polarization of the hair cells produced a transverse motion of the tectorial membrane towards the neural limb (Fig. 7B, 7C). A mean negative displacement of beads of 24 ± 16 nm (range 10 to 56 nm; $d = 0.36 – 0.51$) was achieved in eight preparations using 100 μA current flowing from the abneural to neural electrodes. These measurements were made on beads located above SHCs and, by focusing through the tectorial membrane, it was possible also to image the bundles (Fig. 7A, 7B). Comparison of the relative displacement of the hair bundle to that of beads lying directly above the bundle indicated that the bundle moved slightly more than the bead (Fig. 7B). The ratio of the bundle to bead displacement for the same polarization was 1.45 ± 1.1 (n= 5), though this is not significantly different from 1 (two-tailed Students t-test, $p = 0.2$) suggesting a tight coupling of the bundles to the tectorial membrane. Tectorial membrane motion in response to extracellular stimulation was also monitored over the THCs, the mean negative displacement being 25 ± 22 nm (n= 4).

The displacements obtained by extracellular polarization were similar to those elicited from individual SHCs in that they were reversibly blocked by 10 mM Na^+ salicylate (Fig. 7C). This reversible block, shown in four preparations, makes it unlikely that lateral movements produced by extracellular currents stemmed from a direct electrophoretic motion of the tectorial membrane. The dose-response relationship for the action of salicylate on the voltage-evoked movements (Fig. 7D, 7E) was fit with a Hill equation with a half-blocking concentration of 3.6 mM, similar to that in OHCs (Tunstall et al., 1995). In order to ascertain whether the bundle movements were elicited over the same range of membrane potentials as those seen in individual SHCs, we estimated the membrane depolarization evoked by

extracellular polarization. To do this, SHCs were patch clamped in a preparation in which the tectorial membrane had been removed but which was stimulated by extracellular current polarization (Fig. 7F). The change in membrane potential increased with the current polarization, as did the size of the hair bundle movement. In multiple SHC recordings, the depolarization (measured in current-clamp) was proportional to the magnitude of the external current from 40 to 100 μA, with a proportionality constant of 0.74 mV/ μA. If extracellular current stimuli are as effective in the presence of the tectorial membrane, the 100 μA polarization routinely used would depolarize the SHCs to ~20 mV assuming they have a resting potential of about −55 mV in perilymph (Tan et al., 2013).

Prestin in chicken hair cells

The evidence described so far for the existence of prestin in the chicken papilla is largely circumstantial but the presence of the motor protein was confirmed by RT-PCR and immunolabeling (Fig. 8). Amplification of cDNA derived from the papilla using primers designed against chicken prestin produced a band of the correct size (382 nt) identical to a band produced by amplification of plasmid containing chicken prestin (Fig. 8A). These results confirm the original cloning of prestin from chicken inner ear (Shaechinger and Oliver, 2007; Tan et al., 2011). Localization to the hair cells was demonstrated by immunolabeling with an antibody against an N-terminal peptide sequence of mammalian prestin. Immunoblots of protein extracts of chicken basilar papilla and mouse cochlea labeled with the antibody displayed a principal band at ~80 kDa, appropriate for prestin in both animals (mouse, 81.3 kDa; chicken, 81.1 kDa). Similar results were seen in three other blots. When applied to the papilla, the antibody labeled the lateral membrane of SHCs (Fig. 8C) and THCs (Fig. 8D). Z-projections of the stack (Fig. 8C) showed the label as a ring around the basolateral aspect of the cell; in some SHCs (Fig. 8E, middle) the label was denser on the side where the top of the cell has a lip projecting towards the neural limb. Hair cell bounds were defined by immunolabeling also for otoferlin which is present in the cell membrane and cytoplasm (Goodyear et al. 2010); comparison with the prestin demonstrated that the prestin label was in the hair cell (Fig. 8C, 8E) and none was present in the supporting cells. SHC labeling at other positions confirmed that prestin occurred along the entire epithelium, the label being consistently weaker at the apex ($d = 0.2$) and stronger at the base ($d = 0.8$). We did not quantify the change in labeling intensity with location, but the results suggest a tonotopic gradient in prestin as for other hair cell proteins (Tan et al., 2013).

DISCUSSION

We investigated likely electro-mechanical processes in chicken auditory hair cells by measuring ‘active’ hair bundle motion because this might underlie acoustic amplification and extension of the auditory frequency range in birds. Our main findings were: (1) depolarizing a hair cell elicited biphasic bundle displacements consisting of two processes, one inhibited by MT channel blockers and the other by Na^+ salicylate; (2) salicylate had no effect on the maximum current, gating or adaptation of the MT channels but did block a non-linear capacitance sensitive to the intracellular chloride concentration; (3) hair bundle deflection with a flexible glass fiber could produce a fast bundle ‘recoil’ or ‘mechanical twitch’ that also appeared to possess two components: one observed in voltage-clamp probably reflecting MT channel adaptation (Benser et al., 1996 Ricci et al., 2000) and another recruited by the depolarizing receptor potential; (4) active movements of the bundles were tightly coupled to the tectorial membrane when present indicating they were not solely a feature of free-standing bundles but could exert force in the intact auditory papilla; (5) the lateral membrane around the cuticular plate was labeled with antibodies against prestin. The bundle movements were characterized predominantly in SHCs because their hair bundles

were brighter and better imaged, but most of the processes we describe also exist in THCs. We suggest that the two 'active' processes could sum to function as a negative feedback control on hair bundle position and with fast kinetics might amplify extrinsic mechanical stimuli. They might also underlie the otoacoustic emissions, spontaneous or evoked sound production at the tympanum, which have been recorded in birds (Kettembeil et al., 1995; Burkard et al., 1996; Chen et al., 2001).

Electrically-evoked hair bundle movements were previously reported in chicken hair cells but neither the underlying mechanism nor the link to mechanotransduction was examined (Brix and Manley, 1994). Here, the movements generated by depolarization were generally large, several tens of nanometers in amplitude, and comparable to the working range of the MT channels (52 nm), suggesting they are physiologically significant. They most likely account for the otoacoustic emissions generated by round window electrical stimulation in the chicken ear (Chen et al., 2001). Such emissions were decreased by anoxia and by kanamycin treatment implying they originate with the hair cells. Interestingly, the electrically-evoked emissions have a broad spectrum maximal between 1 kHz and 3 kHz in the upper frequency range of the chicken ear. Our results show that a major component of the electrically-evoked bundle movement was inhibited by salicylate. It was previously found that injection of Na^+ salicylate (5-20 mM) into the avian inner ear had a desensitizing effect by elevating the thresholds of the auditory nerve fibers without changing their characteristic frequency (Shehata-Dieler et al., 1994). Furthermore, this pharmacological action was more pronounced for nerve fibers tuned to higher frequencies of 1 to 3 kHz. Our measurements were confined to the middle region of the papilla which has characteristic frequencies of 0.3 to 0.6 kHz, but the electrically-evoked emissions and salicylate effect suggest such behavior may extend to or become more prominent at higher frequencies. At those frequencies, a hair cell prestin motor may assume greater importance and sharpen the broad passive tuning of the avian basilar membrane (Gummer et al., 1987). At lower characteristic frequencies, the frequency tuning is likely to be dominated by the hair cell electrical resonance (Fuchs et al., 1988; Tan et al., 2013).

Besides the salicylate-sensitive process, there is component attributable to the MT channels, which has been extensively investigated in bullfrog saccular hair cells (Howard and Hudspeth 1988; Benser et al 1996; Martin et al., 2003; Bozovic and Hudspeth 2003) and in turtle auditory hair cells (Crawford and Fettiplace, 1985; Ricci et al., 2000). This component has opposite polarities with respect to bundle motion when elicited by depolarization or hair bundle deflection. One reason for this is that it stems from Ca^{2+}-dependent adaptation of the MT channels and the Ca^{2+} changes differ for the two types of stimuli. During extrinsic deflection of the bundle, stereociliary Ca^{2+} increases causing reclosure of the MT channels thus mediating fast adaptation by translating the current-displacement relationship in the positive direction. But with large depolarization toward the Ca^{2+} equilibrium potential, stereociliary Ca^{2+} is reduced, shifting the current-displacement relationship in the negative direction. Thus with physiological stimuli, the component due to the MT channel and the component sensitive to salicylate will both be negative and could therefore act synergistically (Fig. 6). A consideration of the forces generated by the two processes suggests that at least in the region of papilla studied they are of comparable magnitude. The single-channel gating force can be estimated from the 10-90 percent working range of the current-displacement relationship (Markin and Hudspeth, 1995); for working ranges of 52 nm, the single-channel gating force is 0.32 pN. For mid-frequency SHCs, hair bundles have maximum heights of ~6.0 μm, with about 110 stereocilia/bundle (Tilney and Saunders, 1983) and about 100 tip links, each of which might be attached to two MT channels (Beurg et al., 2009; Tan et al., 2013). Thus, each bundle contains ~200 MT channels supplying a total gating force of 64 pN at the tip of the bundle. The salicylate-sensitive component by comparison can contribute at least 50 pN (Fig. 1B).

The salicylate-sensitive bundle movement is a newly-documented property of chicken hair cells, which, since it can influence neighboring hair bundles, is likely to originate from the cell body. The same size of movements of the tectorial membrane and hair bundles beneath indicates that the force generated by active motion of SHCs might be transmitted via the tectorial membrane to the THCs. The voltage-dependence of the movement, susceptibility to salicylate and presence of a chloride-sensitive non-linear capacitance are all properties redolent of prestin in mammalian OHCs (Ashmore, 2008). We suggest that it is indeed mediated by prestin, antibodies against which labeled the lateral membranes of both SHCs and THCs. By analogy with OHCs, prestin activation by depolarization is likely to cause a shortening of the cell (Ashmore, 2008) but how this is translated into a negative deflection of the hair bundle is unclear. Such an action might be generated if prestin were asymmetrically localized at higher density in the extended neural lip on the SHC, but immunolabeling suggests a fairly uniform distribution around the circumference of the cell. We measured an electrically-evoked displacement of the hair bundle towards the neural limb but it is possible there is also a vertical component of motion perpendicular to the basilar membrane that for SHCs could amplify vibrations of the basilar membrane. However, the transverse motion would be more important functionally as it would facilitate force transfer from hair bundles of SHCs to those of THCs via the tectorial membrane. A possible clue to the origin of the transverse motion is an unusual anatomical feature of the avian hair cells where the cuticular plate runs deep into the cytoplasm and appears to connect to the basolateral membrane facing the neural limb (THCs, Takasaka & Smith, 1971; SHCs, Dieler et al., 1994). With this arrangement, activation of prestin in the basolateral membrane may pull on the cuticular plate and rotate the bundle in the negative direction (Supplementary Fig. S1) accounting for the asymmetry of the motion.

Based on the presence of otoacoustic emissions, there is evidence of an active process in auditory hair cells of lizards as well as birds and mammals (Manley, 2000). For example, the Tokay gecko has prominent otoacoustic emissions which are diminished by salicylate injection (Stewart and Hudspeth, 2000). The most parsimonious explanation for this finding is that lizards too possess a prestin-like mechanism in their auditory hair cells. If so, it strengthens the notion that transformation of the SLC26A5 anion exchanger into a motor protein capable of cochlear amplification was an early development in amniote evolution and not a mammalian invention as is usually supposed. The mammalian step was to free the basolateral membrane from restrictive connections and augment prestin density to enhance the effectiveness of this motor protein.

MATERIALS AND METHODS

Preparation and hair cell recording

Recordings were made from hair cells in the isolated basilar papilla of embryonic (E19-E21) chickens (*Gallus gallus domesticus*, White Leghorn). At these embryonic ages, the frequency range, sensitivity and tonotopic organization all approximate those of mature birds (Jones et al., 2006). Animals were killed by decapitation as approved by the Institutional Animal Care and Use Committee of the University of Wisconsin-Madison according to current National Institutes of Health guidelines. The basilar papilla was isolated (Fuchs et al. 1988; Tan et al. 2013) and the tectorial membrane removed after brief treatment with 0.1 mg/ml of protease type XXIV (Sigma-Aldrich, St. Louis, MO). The isolated papilla was secured in an experimental chamber, hair bundles uppermost, by strands of dental floss on either side of the recording location. The chamber and preparation were transferred to the stage of a Leica DMLFS fixed-stage microscope (Leica Microsystems, Buffalo Grove, IL) and viewed through a long working distance 63X water-immersion objective (numerical aperture 0.9), 2.0X Optivar and Hamamatsu CCD camera. The chamber was perfused with oxygenated saline of composition (in mM): 151 NaCl, 5 KCl, 2.5 (or 1.5) CaCl , 8 Glucose,

2 Na^+ 2 pyruvate, 10 HEPES, pH 7.4 (320 mOsm/l) heated to 33-34°C. Blocking agents (FM1-43; Life Technologies, Grand Island NY; Na^+ salicylate; Sigma-Aldrich; St Louis MO) were introduced via a top perfusion tube or by adding to the bath. SHCs were identified by their abneural location and by their eccentrically-placed hair bundle (Hirokawa, 1978; Fig. 1A). The distance of the recording site from the apical end of the papilla was measured and normalized by the total length of the papilla (~3.6 mm) and is expressed as *d*, the fractional distance from the apex; in most experiments, $d = 0.35 - 0.45$. Hair cell recordings were made with borosilicate patch electrodes filled (except for the non-linear capacitance measurements; see below) with an intracellular solution containing (in mM): 137 KCl, 0.5 BAPTA, 3 MgATP, 10 Tris creatine phosphate, 10 HEPES, pH 7.2 (295 mOsm/l); patch electrodes were connected to an Axopatch 200B amplifier (Molecular Devices, Sunnyvale CA); the residual series resistances was 7.5 ± 3.4 MΩ (n = 40). Membrane potentials were corrected for junction potentials and current flow through the residual series resistance. Unless otherwise noted, the holding potential was −84 mV.

Hair bundle stimulation and imaging

Hair bundles were mechanically stimulated by a fluid jet (Kros et al., 1992) from a pipette, tip diameter ~10 μm, driven by a 25 mm diameter piezoelectric disc (MuRata Electronics, Rockmart GA) or occasionally a stiff glass probe driven by a piezoelectric stack actuator (PA8/12, Piezosystems Jena, Hopedale, MA). In some experiments, hair bundles were deflected with glass fibers more compliant than the hair bundle driven with a piezoactuator. Flexible fibers, ~100 μm long and 0.5 to 1 μm in diameter with stiffness ~1 mN/m, were constructed and calibrated (Ricci et al., 2000) and the tip was placed against the shortest edge of the bundle; hair bundle heights were 6.5 - 5.5 μm at the location studied ($d = 0.35 - 0.45$). The driving voltage to the piezoactuator was filtered at 2 kHz. Bundle motion was determined by projecting an image of the tip of the hair bundle or the end of the flexible fiber near the bundle onto a pair of photodiodes (LD 2-5; Centronics, Newbury Park, CA) at 270X magnification and recording changes in photocurrent, filtered at 2 kHz. Free-standing hair bundles were imaged at their tip where they appeared as a bright line; when flexible fiber stimulation was used, the fiber was placed between a third and a half-way down from the top of the bundle; if too close to the top, it was prone to slip over the bundle during stimulation. The differential photocurrent, proportional to the displacement of the object, was calibrated by measuring its amplitude and polarity when displacing the photodiodes a known distance in the image plane, then using the magnification to determine the equivalent motion in the object plane.

In one set of experiments, the tectorial membrane was not removed and remained attached to the hair bundles. In these experiments, the hair cells were stimulated *en masse* by extracellular currents applied with a stimulus isolation unit (A395; World Precision Instruments, Sarasota, FL) connected to agar-filled glass electrodes contacting chloridized silver wires placed on either side of the papilla. The positive electrode (the anode) was a 20-μm diameter pipette placed ~50 μm from the abneural edge of the papilla whereas the reference electrode was further away on the neural limb side. Movements of the tectorial membrane were measured by imaging 3-μm diameter silica beads (Polyscience, Warrington, PA) that were applied at low density on top of the membrane. For assaying hair bundle motion, responses to 25 to 50 presentations were averaged at each stimulus level. Mechanical and electrical stimuli were generated by automated protocols from a Cambridge Electronic Design (CED; Cambridge, UK) Power1401 interface driven by a PC computer, and data were digitized with the interface and analyzed with IGOR Pro v6 (Wavemetrics, Lake Oswego, OR). Results are presented as the mean ± 1 standard deviation (SD) and significance assessed by two-tailed Student's t test. Relationships between the MT current, I, and hair bundle displacement, X, were fit with a Boltzmann equation: $I = I_{MAX}/(1 + \exp(-$

$(X\text{-}X_O)/X_S)$), where I_{MAX} is the maximum current, X_O the half saturation displacement and X_S the slope factor ; the 10-90 percent working range is given by $4.4 \cdot X_S$.

Non-linear capacitance

Non-linear capacitance measurements were performed in an external saline designed to block all voltage-dependent conductances containing (in mM): NaCl, 136; CsCl, 5; $CaCl_2$, 0.5; $MgCl_2$, 2; $CoCl_2$, 2; tetraethylammonium bromide, 10; 4-aminopyridine, 5; apamin, 0.3 μM; HEPES, 10; glucose 8, pH 7.4 (321 mOsm/l). The patch-electrode solution was similar to that above with the exception that KCl was replaced with CsCl. For reducing intracellular chloride, CsCl was isotonically replaced with Cs^+ aspartate. A continuous measurement of SHC membrane capacitance was obtained (Santos-Sacchi et al., 1998) by applying a voltage clamp protocol consisting of a double sine wave (10 mV peak-to-peak at 391 Hz and at 781 Hz) superimposed on a 200 ms voltage ramp from −150 to +150 mV. Voltage commands and data acquisition were controlled with jClamp (www.SciSoftCo.com). SHC capacitances were determined in the presence and absence of 10 mM Na^+ salicylate and the difference capacitance ΔC_m was derived. The variation of ΔC_m with membrane potential, V, was fit with the first derivative of a two-state Boltzmann function (Santos-Sacchi et al., 1998):

$$\Delta C_m = Q_{\max} \frac{ze}{kT} \frac{\varepsilon}{(1+\varepsilon)^2} \quad (1)$$

where

$$\varepsilon = \exp\left(\frac{(ze\,(V - V_{0.5})}{kT}\right)$$

Boltzmann parameters were evaluated from the fits: Q_{max} (maximum nonlinear charge moved), $V_{0.5}$ (voltage at peak capacitance), and z (valence). In equation 1, e is the electron charge, k is the Boltzmann constant and T is temperature; kT/e = 26.4 mV at 33°C.

RT-PCR and immunolabeling

Chickens were killed by decapitation and basilar papillae isolated (five papillae from E21 and four from E16 birds) and used for extraction of total RNA with the Ambion RNAqueous-4PCR kit (Life Technologies, Rockville, MD, USA). The concentration of RNA for each papilla was ~19 ng/μl at both ages. The RNA was pooled at each age and reverse-transcribed into cDNA using an Improm-II reverse transcription kit (Promega, Madison WI) with a random primer set (Integrated DNA technologies, Coralville, IA). The cDNA was amplified with forward, **tcttgcaaggacagttgcac,** and reverse, **tcaggcacttgtctcacagc**, primers bracketing nucleotides 248-629 in the open reading frame of chicken prestin (GenBank accession number EF028087.1; Schaechinger and Oliver 2007) using Invitrogen Platinum Taq DNA Polymerase (Life Technologies, Grand Island, NY). As a positive control, 200 ng/μl of pEGFP-N1 plasmid containing chicken prestin (Schaechinger and Oliver, 2007; Tan et al., 2011) was also amplified with the same primer set. PCR products were electrophoresed on 1% agarose gel.

A polyclonal antibody against the N-terminal peptide sequence of rat prestin, CKYLVERPIFSHPVLQE (Bethyl Laboratories, Montgomery TX), which is closely homologous to the equivalent sequence in chicken prestin, was used to label the basilar papilla. The antibody was affinity purified and shown to immunolabel rat OHCs (Mahendrasingam et al., 2010). Immunoblots were performed on tissue from fifteen E19 chicken papillae and twelve P11 mice cochleas; mice were decapitated and cochleas

dissected out using procedures approved by the Institutional Animal Care and Use Committee of the University of Wisconsin-Madison. Proteins were extracted with Tissue Extraction Reagent I (Invitrogen Life Technologies) plus protease inhibitor cocktail (Sigma-Aldrich), denatured and electrophoretically separated on a 7.5 % SDS-PAGE and blotted onto a 0.45 μm nitrocellulose membrane. Blotted membranes were incubated with the prestin antibody (1:100 dilution) at 4°C overnight then incubated in secondary goat anti-rabbit horseradish peroxidase-conjugated antibody (1:1000, Invitrogen) for 90 min at room temperature and stained with Novex chemiluminescent reagent.

Chicken papillae were fixed in 4% paraformaldehyde in phosphate buffered saline (PBS) for 30 min, washed then permeabilized with 0.5% Triton-X for 30 min. Fixed papillae were immersed in 10 % goat serum (Invitrogen) for 1h at room temperature and incubated overnight at 4°C with the prestin antibody (dilution 1:50) and the mouse monoclonal HCS-1 antibody (dilution 1:400) which labels otoferlin in chicken hair cells (Goodyear et al., 2010). After rinsing in PBS, specimens were incubated with Alexa Fluor 488 goat anti-rabbit IgG antibody (1:200; Invitrogen) and goat anti-mouse Alexa Fluor 568 for 90 min and Alexa Fluor 647 phalloidin (1:200; Invitrogen Life Sciences) for 60 min at room temperature. Preparations were mounted in Fluoromount-G medium (SouthernBiotech, Birmingham, AL) with cover slips and viewed under a 60X oil-immersion objective (NA = 1.4) on a Nikon A1 laser scanning confocal microscope.

Supplementary Material

Refer to Web version on PubMed Central for supplementary material.

Acknowledgments

Work was supported by grant RO1 DC01362 from the National Institutes on Deafness and other Communication Disorders to RF. We thank Dan Yee for constructing electrical equipment, Ana Garic for assistance with molecular biology, Lance Rodenkirch for advice on confocal imaging, Dominik Oliver for the pEGFP-N1 plasmid containing chicken prestin and Jeff Corwin for the HCS-1 antibody.

References

Amann R, Peskar BA. Anti-inflammatory effects of aspirin and sodium salicylate. Eur. J. Pharmacol. 2002; 447:1–9. [PubMed: 12106797]

Ashmore J. Cochlear outer hair cell motility. Physiol. Rev. 2008; 88:173–210. [PubMed: 18195086]

Benser ME, Marquis RE, Hudspeth AJ. Rapid, active hair bundle movements in hair cells from the bullfrog's sacculus. J. Neurosci. 1996; 16:5629–43. [PubMed: 8795619]

Beurg M, Fettiplace R, Nam J-H, Ricci AJ. Localization of inner hair cell mechano-transducer channels using high-speed calcium imaging. Nature Neurosci. 2009; 12:553–558. [PubMed: 19330002]

Bozovic D, Hudspeth AJ. Hair-bundle movements elicited by transepithelial electrical stimulation of hair cells in the sacculus of the bullfrog. Proc. Natl. Acad. Sci. USA. 2003; 100:958–63. [PubMed: 12538849]

Brix J, Manley GA. Mechanical and electromechanical properties of the stereovillar bundles of isolated and cultured hair cells of the chicken. Hear. Res. 1994; 76:147–57. [PubMed: 7928707]

Burkard R, Salvi R, Chen L. 2f1-f2 distortion product otoacoustic emissions in White Leghorn chickens (Gallus domesticus): effects of frequency ratio and relative level. Audiol. Neurootol. 1996; 1:197–213. [PubMed: 9390802]

Chen L, Sun W, Salvi RJ. Electrically-evoked otoacoustic emissions from the chicken ear. Hear. Res. 2001; 161:54–64. [PubMed: 11744281]

Choe Y, Magnasco MO, Hudspeth AJ. A model for amplification of hair-bundle motion by cyclical binding of Ca2+ to mechanoelectrical-transduction channels. Proc. Natl. Acad. Sci. USA. 1998; 95:15321–6. [PubMed: 9860967]

Crawford AC, Fettiplace R. The mechanical properties of ciliary bundles of turtle cochlear hair cells. J. Physiol. 1985; 364:359–379. [PubMed: 4032304]

Dallos P. Cochlear amplification, outer hair cells and prestin. Curr. Opin. Neurobiol. 2008; 18:370–376. [PubMed: 18809494]

Dieler R, Shehata-Dieler WE, Richter CP, Klinke R. Effects of endolymphatic and perilymphatic application of salicylate in the pigeon. II: Fine structure of auditory hair cells. Hear. Res. 1994; 74:85–98. [PubMed: 8040102]

Fischer FP. Quantitative analysis of the innervation of the chicken basilar papilla. Hear. Res. 1992; 61:167–178. [PubMed: 1526890]

Fuchs PA, Nagai T, Evans MG. Electrical tuning in hair cells isolated from the chick cochlea. J. Neurosci. 1988; 8:2460–7. [PubMed: 3249237]

Gale JE, Marcotti W, Kennedy HJ, Kros CJ, Richardson GP. FM1-43 dye behaves as a permeant blocker of the hair-cell mechanotransducer channel. J. Neurosci. 2001; 21:7013–25. [PubMed: 11549711]

Goodyear RJ, Legan PK, Christiansen JR, Xia B, Korchagina J, Gale JE, Warchol ME, Corwin JT, Richardson GP. Identification of the hair cell soma-1 antigen, HCS-1, as otoferlin. J. Assoc. Res. Otolaryngol. 2010; 11:573–86. [PubMed: 20809368]

Gummer AW, Smolders JW, Klinke R. Basilar membrane motion in the pigeon measured with the Mössbauer technique. Hear. Res. 1987; 2:63–92. [PubMed: 3654398]

He DZ, Beisel KW, Chen L, Ding DL, Jia S, Fritzsch B, Salvi R. Chick hair cells do not exhibit voltage-dependent somatic motility. J. Physiol. 2003; 546:511–20. [PubMed: 12527737]

Hirokawa N. The ultrastructure of the basilar papilla of the chick. J. Comp. Neurol. 1978; 181:361–74. [PubMed: 690270]

Howard J, Hudspeth AJ. Compliance of the hair bundle associated with gating of mechanoelectrical transduction channels in the bullfrog's saccular hair cell. Neuron. 1988; 1:189–99. [PubMed: 2483095]

Hudspeth AJ, Choe Y, Mehta AD, Martin P. Putting ion channels to work: mechanoelectrical transduction, adaptation, and amplification by hair cells. Proc. Natl. Acad. Sci. USA. 2000; 97:11765–72. [PubMed: 11050207]

Jones TA, Jones SM, Paggett KC. Emergence of hearing in the chicken embryo. J. Neurophysiol. 2006; 96:128–41. [PubMed: 16598067]

Kettembeil S, Manley GA, Siegl E. Distortion-product otoacoustic emissions and their anaesthesia sensitivity in the European starling and the chicken. Hear. Res. 1995; 86:47–62. [PubMed: 8567421]

Köppl C. Birds--same thing, but different? Convergent evolution in the avian and mammalian auditory systems provides informative comparative models. Hear. Res. 2011; 273:65–71. [PubMed: 20430083]

Kros CJ, Rüsch A, Richardson GP. Mechano-electrical transducer currents in hair cells of the cultured neonatal mouse cochlea. Proc. Roy. Soc. Biol. Sci. 1992; 249:185–93.

Mahendrasingam S, Beurg M, Fettiplace R, Hackney CM. The ultrastructural distribution of prestin in outer hair cells: a post-embedding immunogold investigation of low-frequency and high-frequency regions of the rat cochlea. Eur. J. Neurosci. 2010; 31:1595–605. [PubMed: 20525072]

Manley GA. Cochlear mechanisms from a phylogenetic viewpoint. Proc. Natl. Acad. Sci. USA. 2000; 97:11736–43. [PubMed: 11050203]

Manley GA, Köppl C. Phylogenetic development of the cochlea and its innervation. Curr. Opin. Neurobiol. 1998; 8:468–474. [PubMed: 9751658]

Marcotti W, van Netten SM, Kros CJ. The aminoglycoside antibiotic dihydro-streptomycin rapidly enters mouse outer hair cells through the mechano-electrical transducer channels. J. Physiol. 2005; 567:505–21. [PubMed: 15994187]

Markin VS, Hudspeth AJ. Gating-spring models of mechanoelectrical transduction by hair cells of the internal ear. Annu. Rev. Biophys. Biomol. Struct. 1995; 24:59–83. [PubMed: 7663129]

Martin P, Bozovic D, Choe Y, Hudspeth AJ. Spontaneous oscillation by hair bundles of the bullfrog's sacculus. J. Neurosci. 2003; 23:4533–48. [PubMed: 12805294]

Murrow BW. Position-dependent expression of potassium currents by chick cochlear hair cells. J. Physiol. 1994; 480:247–59. 1994. [PubMed: 7869243]

Oliver D, He DZ, Klöcker N, Ludwig J, Schulte U, Waldegger S, Ruppersberg JP, Dallos P, Fakler B. Intracellular anions as the voltage sensor of prestin, the outer hair cell motor protein. Science. 2001; 292:2340–3. [PubMed: 11423665]

Ricci AJ, Crawford AC, Fettiplace R. Active hair bundle motion linked to fast transducer adaptation in auditory hair cells. J. Neurosci. 2000; 20:7131–42. [PubMed: 11007868]

Santos-Sacchi J. Reversible inhibition of voltage-dependent outer hair cell motility and capacitance. J. Neurosci. 1991; 11:3096–110. [PubMed: 1941076]

Santos-Sacchi J, Kakehata S, Takahashi S. Effects of membrane potential on the voltage dependence of motility-related charge in outer hair cells of the guinea-pig. J. Physiol. 1998; 510:225–235. [PubMed: 9625879]

Schaechinger TJ, Oliver D. Nonmammalian orthologs of prestin (SLC26A5) are electrogenic divalent/chloride anion exchangers. Proc. Natl. Acad. Sci. USA. 2007; 104:7693–8. [PubMed: 17442754]

Shehata-Dieler WE, Richter CP, Dieler R, Klinke R. Effects of endolymphatic and perilymphatic application of salicylate in the pigeon. I: Single fiber activity and cochlear potentials. Hear. Res. 1994; 74:77–84. [PubMed: 8040101]

Stewart CE, Hudspeth AJ. Effects of salicylates and aminoglycosides on spontaneous otoacoustic emissions in the Tokay gecko. Proc. Natl. Acad. Sci. USA. 2000; 97:454–9. [PubMed: 10618439]

Sul B, Iwasa KH. Effectiveness of hair bundle motility as the cochlear amplifier. Biophys. J. 2009; 97:2653–63. [PubMed: 19917218]

Szymko YM, Dimitri PS, Saunders JC. Stiffness of hair bundles in the chick cochlea. Hear. Res. 1992; 59:241–9. [PubMed: 1618714]

Tan X, Pecka JL, Tang J, Okoruwa OE, Zhang Q, Beisel KW, He DZ. From zebrafish to mammal: functional evolution of prestin, the motor protein of cochlear outer hair cells. J. Neurophysiol. 2011; 105:36–44. [PubMed: 21047933]

Tan X, Beurg M, Hackney CM, Mahendrasingam S, Fettiplace R. Electrical tuning and transduction in short hair cells of the chicken auditory papilla. J. Neurophysiol. 2013; 109:2007–20. [PubMed: 23365177]

Takasaka T, Smith CA. The structure and innervation of the pigeon's basilar papilla. J. Ultrastruct. Res. 1971; 35:20–65. [PubMed: 4102964]

Tilney LG, Saunders JC. Actin filaments, stereocilia, and hair cells of the bird cochlea. I. Length, number, width, and distribution of stereocilia of each hair cell are related to the position of the hair cell on the cochlea. J. Cell. Biol. 1983; 96:807–21. [PubMed: 6682110]

Tunstall MJ, Gale JE, Ashmore JF. Action of salicylate on membrane capacitance of outer hair cells from the guinea-pig cochlea. J. Physiol. 1995; 485:739–752. [PubMed: 7562613]

Zheng J, Shen W, He DZ, Long KB, Madison LD, Dallos P. Prestin is the motor protein of cochlear outer hair cells. Nature. 2000; 405:149–155. [PubMed: 10821263]

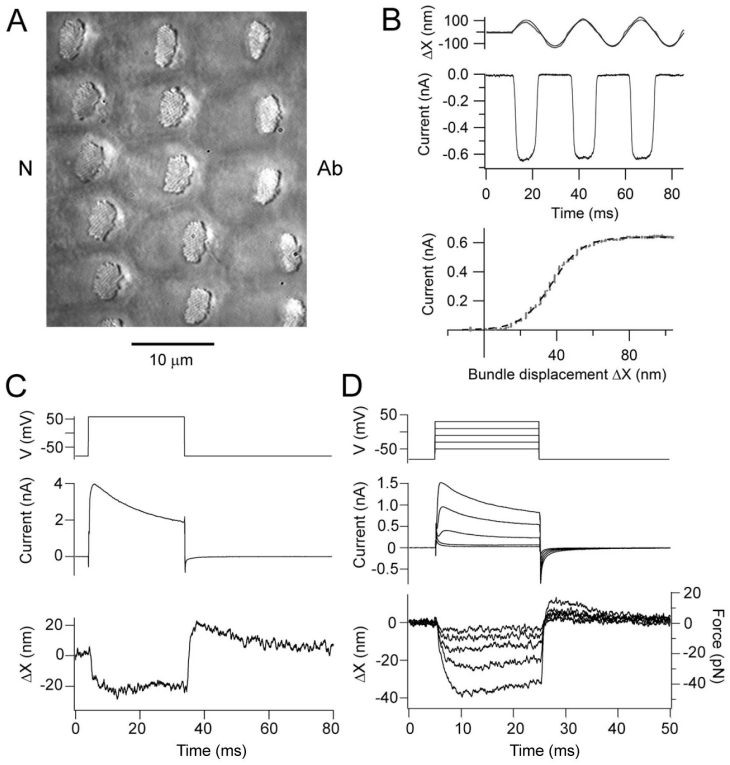

Figure 1.

Mechanotransduction and hair bundle movements in chicken SHCs. (A) Surface view of chicken basilar papilla showing the hair bundles of SHCs, orientation indicated by Ab (abneural) and N (neural) sides. Note the bundles are eccentrically located towards the abneural edge of papilla. (B) MT currents in response to saturating bundle motion elicited by sinusoidal fluid jet stimuli. In the stimulus monitor (top) the thin line is the calibrated photodiode current superimposed on the driving voltage to the fluid jet piezoelectric disk. The MT current throughout the first cycle is plotted against bundle displacement, ΔX (bottom) and is fitted with a Boltzmann equation (dashed line) with I_{MAX} of −0.64 nA and 10-90 per cent working range (see Methods) of 37 nm. In this and subsequent current-displacement relations, the absolute amplitude of the current is plotted. (C) Depolarizing voltage step (top) from −84 to +56 mV generates a partially inactivating membrane current (middle) and a deflection of a free-standing bundle (bottom) which is predominantly negative (away from the tallest edge of the bundle). (D) Set of depolarizing voltage steps in another SHC generates negative bundle movements graded with the depolarization. In this case, a flexible glass fiber, stiffness 1.2 mN/m, was attached to the hair bundle allowing calculation of forces produced (bottom, right hand axis).

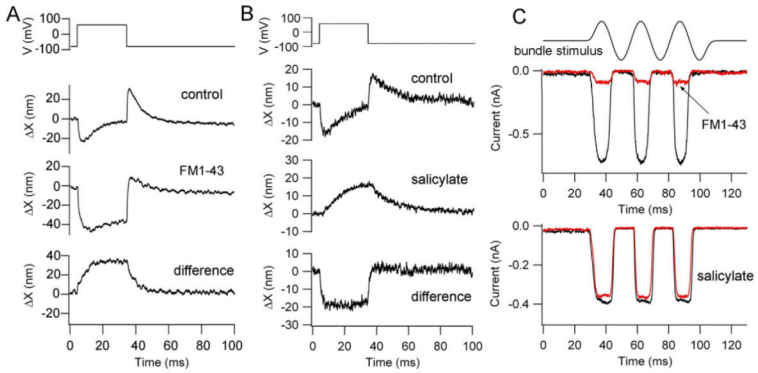

Figure 2.

Two components of the voltage-induced hair bundle motion. (A) Depolarization from −84 to +56 mV evoked biphasic bundle motion. The MT channel blocker FM1-43 (7.5 μM) blocked a positive component of the motion thereby increasing the negative component. The difference motion (control – FM1-43), reflecting the MT channel component is entirely positive (towards abneural edge). (B) The same depolarization in another SHC elicited a biphasic bundle motion that became positive and sustained with application of 10 mM Na^+ salicylate. The difference motion (control - salicylate) is entirely negative (away from bundle's tallest edge). (C) MT currents in these same two SHCs. Top is SHC in (A) without (black trace) and with (red trace) FM1-43 which blocks 90 per cent of the current. Bottom is SHC in (B) without (black trace) and with (red trace) salicylate.

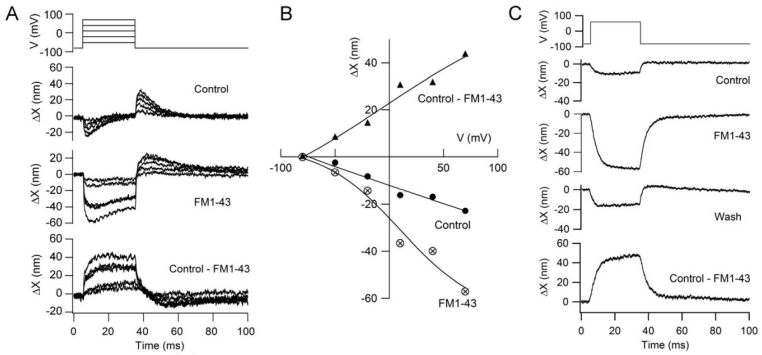

Figure 3.

Action of FM1-43 on voltage-induced bundle motion in a THC. (A) Depolarizing voltage steps from −84 mV to +60 mV evokes biphasic bundle movements which with 7.5 μM FM1-43 become largely negative. The difference motion, (control – FM1-43) is sustained and positive. (B) Voltage dependence of peak displacements for the two processes: owing to block of the positive component by FM1-43, the negative component (crossed circles) increased with application of the MT channel blocker; the difference motion (filled triangles) was positive and both increase with depolarization. Results with FM1-43 fit with a Boltzmann equation $\Delta X = \Delta X_{max} /(1 + \exp((V_{0.5}-V)/ \alpha))$ with $V_{0.5} = 10$ mV, $\alpha = 37$ mV and $\Delta X_{max} = -70$ nm, where V is membrane potential. (C) Effect of 7.5 μM FM1-43 in a SHC showing recovery of the control amplitude of the voltage-evoked bundle movement on washing.

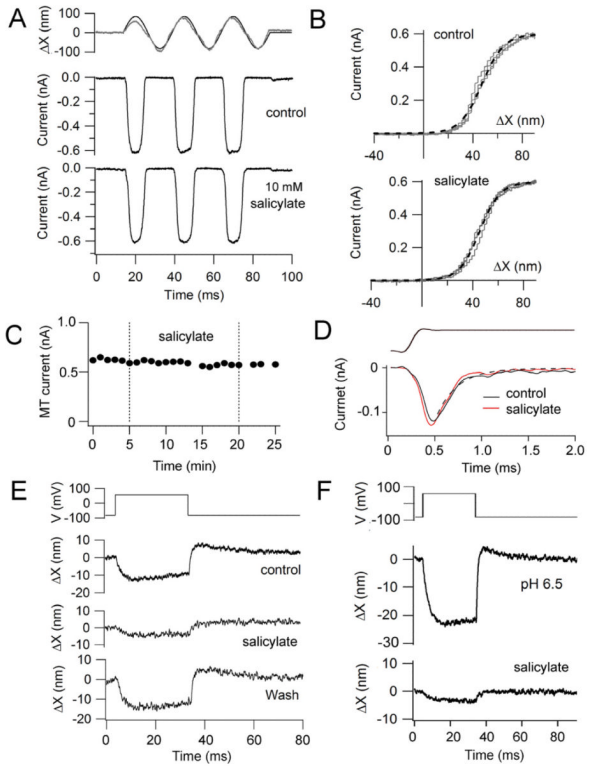

Figure 4.

MT currents in SHCs are unaffected by salicylate. (A) MT currents before (control) and 18 minutes after application of 10 mM Na^+ salicylate to the bath. (B) Current displacement relationships for the responses in (A), each fit with a single Boltzmann (dashed line) with I_{MAX} and 10 – 90 percent working range of 0.6 nA and 39 nm (control) and 0.6 nA and 36 nm (salicylate). (C). Peak MT current versus recording time, 10 mM Na^+ salicylate was bath applied between 5 and 20 minutes. Records in (A) obtained during the initial control and 13 minutes after salicylate application. (D). Onset of MT current in a SHC in response to step deflections of the hair bundle with a stiff glass probe; low-level stimuli evoke fast adaptation that is unaffected by application of 10 mM Na^+ salicylate; currents fit (dashed line) with an adaptation time constant of 0.23 ms, time course of bundle deflection being shown at top. (E) Voltage-evoked hair bundle movements for the cell in (A – C) showing initial control, reduction in 10 mM Na^+ salicylate and full recovery. (F) Voltage-induced bundle motion in another SHC recorded with pipette solution at pH 6.5, before and after application of 10 mM Na^+ salicylate.

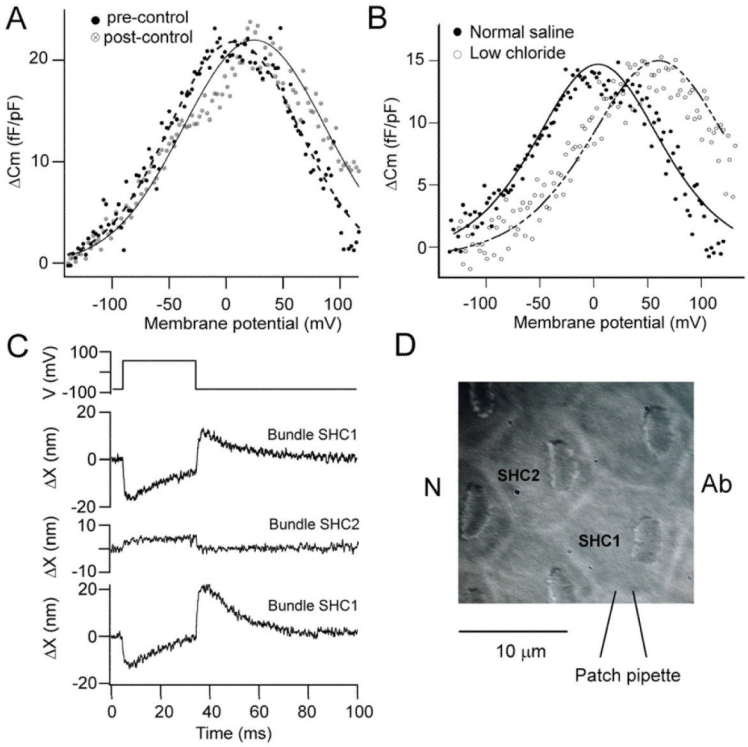

Figure 5.

SHC properties linked to voltage-evoked bundle motion. (A) Non-linear capacitance in a SHC determined (see Methods) as the difference, ΔC_m, between membrane capacitance without and with perfusion of 10 mM Na^+ salicylate. Pre- and post-controls were obtained by using the control prior to salicylate application (filled circles) and the wash after salicylate (open circles) for the subtraction and indicate full recovery from the salicylate. The ordinate is scaled by the linear capacitance, 6.4 pF. Each set of points was fit with equation 1, with $V_{0.5}$ = 7 mV, z = 0.71 (filled circles) and $V_{0.5}$ = 25 mV, z = 0.63 (open circles) and ΔC_m = 22 fF/pF for both. (B) Non-linear capacitance in two SHCs recorded with normal intracellular saline containing 161 mM Cl^- (filled circles) and low Cl^- in which all but 20 mM CsCl was replaced by Cs^+ aspartate (open circles). Points fit with equation 1, with $V_{0.5}$ = 4 mV, z = 0.57, linear capacitance = 5.7 pF (normal) and $V_{0.5}$ = 60 mV, z = 0.62, linear capacitance = 5.5 pF (low Cl^-). Note positive voltage shift with low Cl^- intracellular. (C). Voltage-induced hair bundle motion in patch clamped cell, SHC1, and in adjacent cell, SHC2 (not clamped), with return control from original cell SHC1. Bundle motion of nearby SHC suggests force generation in cell body or cuticular plate. Polarity and magnitude of bundle motion obtained by sequential calibration of bundle-1 and bundle-2 images. (D). Schematic of experiments in (C), polarity, Ab (abneural) and N (neural) sides of papilla.

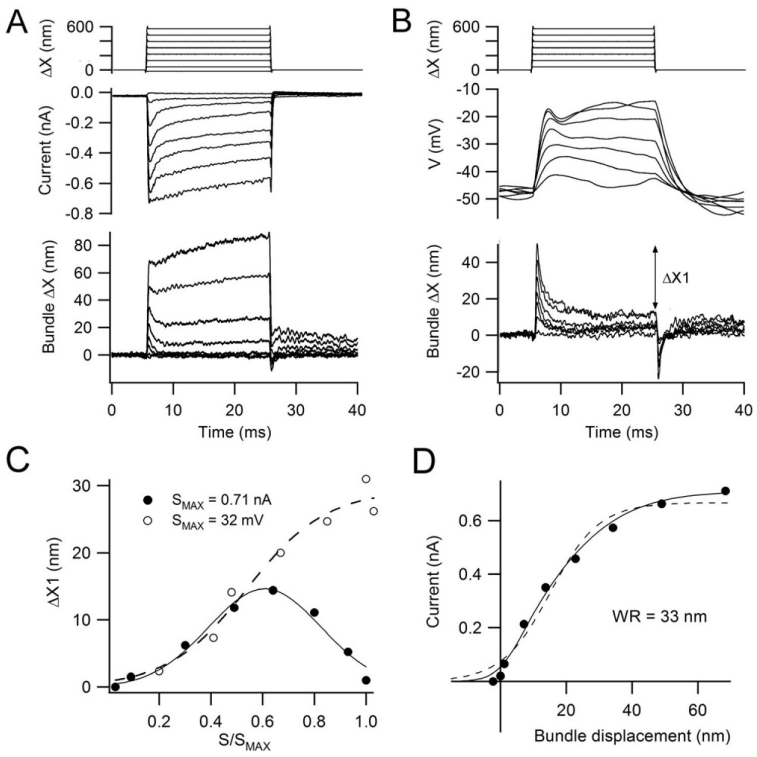

Figure 6.

SHC hair bundle deflection with a flexible fiber. (A) MT currents for step deflections of a flexible fiber: top, motion of proximal end of fiber attached to piezoactuator; middle, MT currents recorded under voltage clamp at −84 mV holding potential; bottom, motion of distal end of fiber which contacted the neural edge of the hair bundle. Note the initial notch on the bundle displacement, appearing as an apparent time-dependent increase in stiffness. (B) Receptor potentials in the same SHC recorded under current-clamp from a resting potential of −48 mV. Top and bottom traces as in (A); note the larger size of the notch or recoil in the bundle displacement. The recoil was quantified by the displacement difference, ΔX1, between the initial peak and the steady state. (C) Size of recoil, ΔX1, in the voltage-clamp (filled circles) and the current-clamp experiments (open circles). ΔX1 is plotted against the MT current or receptor potential, S, normalized to their respective maximum values, S_{MAX} = 0.71 nA or 32 mV. (D) Current-displacement relationship from records in (A), peak current plotted against peak displacement. Points fitted with a single Boltzmann equation (dashed line) with I_{MAX} = 0.65 nA, 10 – 90 percent working range = 33 nm. Improved fit was obtained with a double Boltzmann equation (continuous line), $I = I_{MAX}/(1 + \{\exp(-(\Delta X\text{-}3)/3)\}\{1 + \exp(-(\Delta X - 14)/12)\})$ where I is the MT current, I_{MAX} = 0.71 nA, ΔX is bundle displacement and numbers in exponents are in nm.

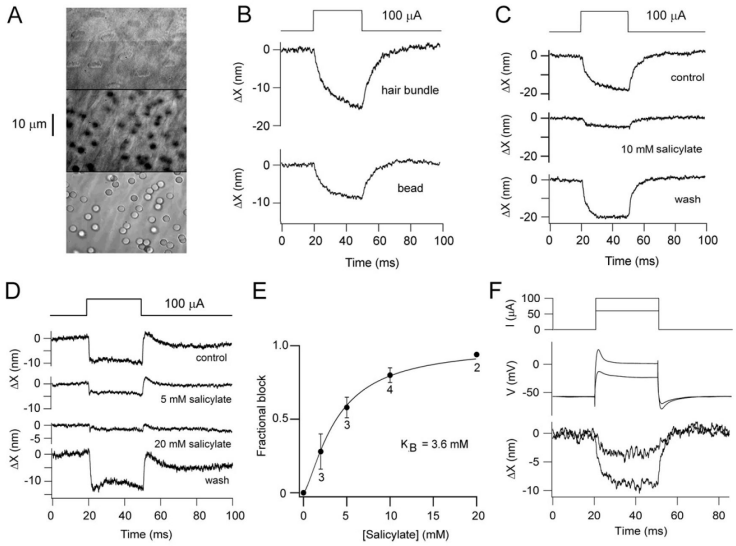

Figure 7.

Voltage-induced motion of tectorial membrane. (A) Images at different focal planes from SHC hair bundles (top) to surface of tectorial membrane (bottom) with 3-μm silica beads attached. Middle image shows transverse fibers of the tectorial membrane and out of focus beads. (B) Displacement of hair bundle and bead on tectorial membrane in response to extracellular current injection. (C) Displacement of bead on tectorial membrane in absence (control and recovery) and presence of 10 mM Na^+ salicylate. (D) Tectorial membrane movements in control, 5 mM and 20 mM Na^+ salicylate and recovery; each trace generated by subtraction of the MT current component determined by application of 8 μM FM1-43. (E) Mean fractional block (± 1 standard deviation) of tectorial membrane motion versus salicylate concentration, number of measurements beside points; dose-response relationship fit with a Hill equation with half-blocking concentration K_B = 3.6 mM and Hill coefficient 1.4. (F) Calibration of extracellular current stimuli (60 and 100 A; top) by simultaneous recording of SHC membrane potential (middle) and hair bundle motion (bottom) in a preparation without a tectorial membrane.

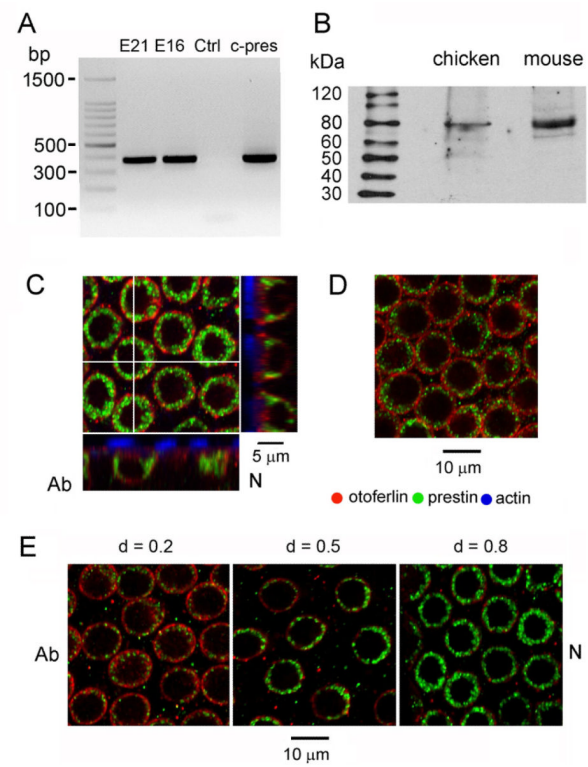

Figure 8.

Prestin in the chicken papilla. (A) RT-PCR products from amplification with chicken prestin primers: lane 1, E21 papilla; lane 2, E16 papillae; lane 3, no cDNA; lane 4, pEGFP-N1 plasmid containing chicken prestin. The predicted product size is 382 base pairs. (B) Immunoblot of chicken basilar papillar and mouse cochlear extracts labeled with the N-terminal prestin antibody used on tissue shows for both animals a principal band ~80 kDa as expected for prestin. Lanes loaded with 140 μg of chicken protein extract and 84 μg of mouse protein (C) Confocal section (0.8 μm full-width at half-maximum) from SHC stack at the level of the nucleus; z-projections, denoted by white cross lines, shown at the right and bottom; hair bundle actin (phalloidin, blue), otoferlin (HCS-1, red), prestin (green); $d = 0.8$. (D) Confocal section of THCs, evident by higher packing density; $d = 0.55$. (E) Confocal sections at SHC nucleus level for locations $d = 0.2$, 0.5 and 0.8; all images from the same preparation under identical acquisition settings. Labeling increased from apex to base; section orientations, N (neural), Ab (abneural).